Published in final edited form as:
Mol Cancer Ther. 2013 June ; 12(6): 992–1001. doi:10.1158/1535-7163.MCT-12-0995.

BIBF 1120 (Nintedanib), a triple angiokinase inhibitor, induces hypoxia but not EMT and blocks progression of preclinical models of lung and pancreatic cancer

Bercin Kutluk Cenik[1], **Katherine T. Ostapoff**[1,2], **David E. Gerber**[3,*], and **Rolf A. Brekken**[1,2,4,*]

[1]Hamon Center for Therapeutic Oncology Research, University of Texas Southwestern Medical Center, Dallas, TX 75390-8593

[2]Division of Surgical Oncology, Department of Surgery, University of Texas Southwestern Medical Center, Dallas, TX 75390-8593

[3]Division of Hematology and Oncology, Department of Internal Medicine, University of Texas Southwestern Medical Center, Dallas, TX 75390-8593

[4]Department of Pharmacology, University of Texas Southwestern Medical Center, Dallas, TX 75390-8593

Abstract

Signaling from other angiokinases may underlie resistance to vascular endothelial growth factor (VEGF)-directed therapy. We evaluated the anti-tumor and biological effects of BIBF 1120 (nintedanib), a tyrosine kinase inhibitor that targets VEGF receptor (VEGFR), platelet-derived growth factor receptor (PDGFR), and fibroblast growth factor receptor (FGFR), in preclinical models of lung and pancreatic cancer, including models resistant to VEGF-targeted treatments. *In vitro,* BIBF 1120 did not show anti-proliferative effects; nor did it sensitize tumor cells to chemotherapy. However, *in vivo* BIBF 1120 inhibited primary tumor growth in all models as a single agent and in combination with standard chemotherapy. Analysis of tumor tissue post treatment revealed that BIBF 1120 reduced proliferation (phospho-histone 3) and elevated apoptosis (cleaved caspase 3) to a greater extent than chemotherapy alone. Furthermore, BIBF 1120 showed potent anti-angiogenic effects, including decreases in microvessel density (CD31), pericyte coverage (NG2), vessel permeability and perfusion, while increasing hypoxia. Despite the induction of hypoxia, markers of epithelial to mesenchymal transition (EMT) were not elevated in BIBF 1120-treated tumors. In summary, BIBF 1120 demonstrated potent anti-tumor and anti-angiogenic activity in preclinical models of lung and pancreatic cancer where it induced hypoxia but not EMT. The absence of EMT induction, which has been implicated in resistance to anti-angiogenic therapies, is noteworthy. Together, these results warrant further clinical studies of BIBF 1120.

Keywords

angiogenesis; lung cancer; pancreatic cancer; vascular endothelial growth factor receptor; fibroblast growth factor receptor; platelet-derived growth factor receptor

[*]Corresponding authors: Rolf A. Brekken, PhD, Hamon Center for Therapeutic Oncology Research, UT Southwestern, 6000 Harry Hines Blvd., Dallas, TX 75390-8593, Tel: 214.648.5151, rolf.brekken@utsouthwestern.edu. David E. Gerber, MD, Simmons Cancer Center, UT Southwestern, 5323 Harry Hines Blvd., Dallas, TX 75390-8852, Tel: 214.648.4180, david.gerber@utsouthwestern.edu.

Disclosure of Potential Conflicts of Interest

R.A. Brekken and D.E. Gerber: commercial research grant from Boerhringer Ingelheim.

Introduction

Despite initial promise and sound biologic rationale, anti-angiogenic therapies targeting vascular endothelial growth factor (VEGF) have demonstrated only modest clinical effect and are prone to resistance in many disease contexts (1). In advanced non-small cell lung cancer (NSCLC), the anti-VEGF monoclonal antibody bevacizumab increases overall survival from approximately 10 to 12 months when added to carboplatin-paclitaxel chemotherapy (2), but conveys no survival benefit when added to cisplatin-gemcitabine chemotherapy (3). The addition of sorafenib, a VEGF receptor (VEGFR) tyrosine kinase inhibitor, to standard chemotherapy does not improve clinical outcomes and is associated with inferior outcomes in tumors with squamous histology (4). In advanced pancreatic cancer, the addition of bevacizumab to gemcitabine does not improve overall survival (5).

In tumors such as lung and pancreatic cancers, proliferation and growth signaling through alternate angiogenic pathways, such as platelet-derived growth factor (PDGF) (6, 7) and fibroblast growth factor (FGF) (8), appears to participate in tumor escape from anti-VEGF therapy. The PDGF-PDGFR axis effects angiogenesis, fibroblast activation, and tumor interstitial pressure (9). In NSCLC, expression of FGF and PDGF are associated with poor prognosis (10). Similar associations have been observed in pancreatic cancer (11).

Based on these observations, it follows that targeting multiple angiokinases would be a logical therapeutic approach (6, 12). However, most available drugs feature an imbalanced pharmacodynamic profile that may result in toxicities precluding optimal inhibition of key pathways (13), particularly the FGF-FGFR axis. Sorafenib, sunitinib, pazopanib, and cediranib have IC_{50}s for FGFR that range 7–25 times greater than IC_{50}s for VEGFR, 2–40 times greater than IC_{50}s for PDGFR, and 2–300 times greater than IC_{50}s for cKIT (inhibition of which can result in myelosuppression). Indeed, the FGFR IC_{50}s achieved with sorafenib (580 nM), sunitinib (2900 nM), and vandetanib (3600 nM) are likely greater than clinically sustainable drug concentrations. By contrast, the pharmacodynamic profile of the receptor tyrosine kinase inhibitor BIBF 1120 (nintedanib, Boehringer Ingelheim) provides balanced inhibition of relevant therapeutic targets: VEGFRs 1, 2, 3 (IC_{50} 13–34 nM); FGFRs 1, 2, 3 (IC_{50} 37–108 nM); and PDGFR α and β (IC_{50} 59–65 nM). Additional targets of BIBF 1120 include FLT-3 and members of the Src-family (Src, Lyn, and Lck), but there is no meaningful inhibition of cKIT (14).

Although BIBF 1120 has demonstrated negligible *in vitro* anti-tumor activity, in animal models single agent BIBF 1120 decreases growth of head and neck, kidney, ovarian, lung, colorectal, prostate, and liver cancer xenografts (14, 15), suggesting that *in vivo* efficacy is due to anti-stromal effects. To evaluate this hypothesis, we studied the effects of BIBF 1120 on tumor growth, metastatic potential, and stromal and vascular parameters in lung cancer and pancreatic cancer models, including selected tumors resistant to anti-VEGF therapies.

Materials and Methods

Cell lines

Human pancreatic cancer lines AsPC-1, HPAF-II, MIA PaCa-2 and the lung cancer line A549 were obtained from the American Type Culture Collection (ATCC). The pancreatic cancer line Colo357 was a gift from Dr. Jason Fleming (Department of Surgical Oncology, MD Anderson Cancer Center, Houston, TX). Lung cancer lines Calu-3, Calu-6, H1703, and H1993 were kindly provided by Dr. John Minna (UT Southwestern). All cell lines were grown in a humidified atmosphere with 5% CO_2, at 37°C, DNA fingerprinted for provenance using the PowerPlex 1.2 kit (Promega), and confirmed to be the same as the DNA fingerprint library maintained by ATCC and the Minna/Gazdar lab. Additionally, they

were confirmed to be free of mycoplasma by e-Myco kit (Boca Scientific) prior to injection into mice.

In vitro cytotoxicity and drug response assay

Cell proliferation assays were performed in 96-well format as described (16). For gemcitabine (Eli Lilly and Company), gemcitabine-BIBF 1120 or gemcitabine-cisplatin-BIBF 1120 the highest dose of gemcitabine administered was 2,000 nmol/L. For cisplatin (APP Pharmaceuticals, co-diluted with gemcitabine) or gemcitabine-cisplatin-BIBF 1120 the highest dose of cisplatin administered was 140 nmol/L. For BIBF 1120 alone, the highest dose was 25.6 μmol/L. For combination studies, a fixed concentration of BIBF 1120 (225 nmol/L) was added to serial dilutions of gemcitabine or gemcitabine plus cisplatin. Relative cell number was calculated on Day 5 by adding the MTS reagent (Promega, final concentration: 333 μg/mL), incubating for 1 to 3h at 37 °C, and reading absorbance in a 490 nm plate reader (Spectra Max 190, Molecular Devices). Drug sensitivity curves and IC_{50} values were calculated using in-house software.

Animal studies

All animals were housed in a pathogen-free facility with continuous access to food and water. Experiments were approved by and performed in accordance with the Institutional Animal Care and Use Committee at the University of Texas Southwestern. Mice were purchased from the core breeding facility at UT Southwestern. Six- to eight-week-old female NOD/SCID mice were injected with 2.5×10^6 lung (A459, Calu-6, H1993) or 1×10^6 pancreatic (HPAF-II, MIA PaCa-2, AsPC-1) cancer cells. Lung cancer cells were injected subcutaneously. Pancreatic cancer cells were injected orthotopically, as described (17). Subcutaneous lung tumor volumes were followed by twice weekly measurements with Vernier calipers. Pancreas tumors were followed by palpation and, if necessary, by ultrasound. Animals were randomized and treatment was initiated as indicated.

BIBF 1120 was suspended in 0.5% hydroxy-ethylcellulose (HEC) as described (14) and administered at a dose of 50 mg/kg 5 days a week via oral gavage. In lung cancer models gemcitabine was administered twice weekly at a dose of 25 mg/kg (i.p.) and cisplatin was administered once weekly at a dose of 1 mg/kg (i.p.). For the pancreas model, gemcitabine was administered at a dose of 12.5 mg/kg (i.p.) 3 times per week. Animals were sacrificed when the average volume of control-treated tumors reached 1500 mm^3 or when animals became moribund.

Perfusion and hypoxia studies

Perfusion studies with labeled dextrans—3 mice per group were injected intravenously with a 1:1 mixture of FITC-conjugated dextran (25 mg/ml, 2×10^6 kDa, Molecular Probes/Invitrogen) and Rhodamine B-conjugated dextran (12.5 mg/ml, 1×10^4 kDa, Molecular Probes/Invitrogen) in 0.9% saline in a volume of 200 μl. The probes were allowed to circulate for 10 minutes. Afterwards, animals were sacrificed, tissues were removed, snap-frozen, embedded in OCT, and 8 μm sections were cut and evaluated as described (18).

Hypoxia studies with pimonidazole—3 mice/group were injected intravenously with 60 mg/kg of pimonidazole (30 mg/ml in 0.9% saline, Hypoxyprobe Plus, HPI Inc.) that was allowed to circulate for 90 minutes before sacrificing animals. Frozen tissue sections were interrogated with FITC-conjugated anti-pimonidazole primary antibody (Chemicon) and endothelial cell markers (CD31, Dianova; Meca-32, DSHB; or Endomucin, Santa Cruz) as described (18). Eight images per tissue area were obtained and analyzed using NIS Elements.

Drug delivery studies with Doxorubicin—3 mice per group from the acute and chronic AsPC-1 endpoint study were injected intravenously with 20 mg/kg Doxorubicin (Johnson & Johnson Pharmaceuticals). Doxorubicin was allowed to circulate for 5 minutes before sacrificing animals. Frozen tissue sections were stained with endothelial cell markers, and visualized under fluorescent microscopy and analyzed as above.

Histology

Tissues were fixed in 4% formalin, embedded in paraffin, sectioned and stained with routine H&E or used for immunohistochemstry. After routine deparaffinization tissue sections were incubated in primary antibody overnight at 4°C. Primary antibodies were used at 5 – 10 μg/ml (see Supplementary Table 1 for complete list of antibodies). Detection with appropriate secondary antibodies and imaging was as described (18).

Statistical analysis

Quantification of immunohistochemistry was performed using NIS Elements 3.2 software (Nikon Instruments). All data was analyzed using GraphPad Prism 5.0 software (GraphPad Software Inc). Data sets were analyzed by student's *t*-test or ANOVA followed by Dunn's post-test and results were considered as significant at $p<0.05$. Results are shown as mean ± SEM. Notation on graphs is as following: *, p<0.05; **, p<0.01; ***, p<0.001; and ****, p<0.0001.

Results

BIBF 1120 does not have anti-proliferative effects, and does not sensitize tumors cells to chemotherapy *in vitro*

We performed cellular proliferation assays in selected lung and pancreatic cancer cell lines using BIBF 1120 as a single agent and in combination with standard of care chemotherapy. As monotherapy, BIBF 1120 did not demonstrate cytotoxic effects, nor did it sensitize the majority of cell lines to chemotherapy (Supplementary Table 2). Single-agent BIBF 1120 had IC_{50} values >20 μmol/L, which are above the pharmacologically achievable concentration in mammals (200–450 nmol/L (14)). In combination studies, a fixed concentration (225 nmol/L) of BIBF 1120 did not alter the cytotoxicity of chemotherapy in A549, Calu-3, Calu-6, H1993, AsPC-1, Colo357, or MIA PaCa-2 cells. However, BIBF 1120 induced a significant shift in the IC_{50} of chemotherapy in H1703 and HPAF-II cells (Supplementary Table 2).

BIBF 1120 inhibits growth of subcutaneous lung xenografts

The *in vivo* efficacy of BIBF 1120, as a single agent and in combination with chemotherapy, was evaluated in SCID mice bearing subcutaneous human lung xenografts (A549, Calu-6 and H1993). Cell lines were selected based on prior knowledge of sensitivity to chemotherapy and anti-angiogenic therapy. For example, we have found A549 to be poorly responsive to bevacizumab (19) and resistant to gemcitabine and cisplatin *in vivo* (20). Calu-6 also responds poorly to bevacizumab but is sensitive to chemotherapy. H1993 is sensitive to bevacizumab and chemotherapy (20).

We initiated single-agent therapy studies with A549 xenografts when primary tumors were less than 200 mm^3 or larger than 250 mm^3. BIBF 1120 effectively reduced primary tumor size in each setting (Supplementary Fig. 1A). To extend these observations we pursued combination therapy studies in A549, H1993, and Calu-6 xenografts. Therapy with vehicle (control), BIBF 1120, chemotherapy, or BIBF 1120 plus chemotherapy commenced when tumors were established. A decrease in tumor growth rate was observed across all models,

particularly in the combination groups, where the growth curve gradually became linear (Fig. 1B).

End tumor volumes and weights were lower in BIBF 1120 and the combination groups compared to controls, across all models ($p<0.0001$, ANOVA, Fig. 1B). In A549 and H1993 xenografts, combination was more effective than single agent therapy ($p<0.001$ and $p<0.01$ respectively, Dunn's post-test, Fig. 1C); however, in Calu-6 xenografts combination therapy was not different from BIBF 1120 single agent therapy.

We next investigated whether the reduction in primary tumor size could be attributed to changes in tumor cell viability *in vivo*. To assess apoptosis and proliferation in these models, tumors were evaluated immunohistochemically for cleaved caspase 3 and phospho-histone H3. This analysis showed a decrease in proliferation (phospho-histone H3) and an increase in apoptosis (cleaved caspase 3) in two lung cancer models (Supplementary Figure 2A–D, data not shown for Calu-6).

BIBF 1120 inhibits growth of orthotopic pancreatic xenografts

Pancreatic cancer cells (HPAF-II, MIA PaCa-2 and AsPC-1) were injected orthotopically into SCID mice. The efficacy of BIBF 1120 as a single agent or in combination with chemotherapy was assessed. *In vitro* the cell lines selected showed differential response to gemcitabine but were not affected by BIBF 1120 (Supplementary Table 2). However, *in vivo* BIBF 1120 significantly reduced tumor size as a single agent in each model and enhanced the activity of gemcitabine in HPAF-II and MIA PaCa-2 xenografts (Fig. 1D).

As observed in A549 xenografts, BIBF 1120 alone or in combination with chemotherapy induced a striking increase in apoptosis (cleaved caspase 3) and decrease in proliferation (phosphorylated histone H3) in Mia-PaCa-2 (Supplementary Figure 2E) and HPAF-II xenografts (data not shown). Gemcitabine treatment alone had little effect on either measure.

BIBF 1120 decreases metastatic burden in pancreatic cancer models

The orthotopic pancreatic cancer models also provided means to assess the effect of BIBF 1120 on metastatic burden. Gross metastatic events counted at sacrifice (which included liver, spleen, peritoneum, lymph node, diaphragmatic and gastrointestinal metastatic foci) were decreased in BIBF 1120-treated animals (Fig. 2). In the chemotherapy combination studies (HPAF-II, MIA PaCa-2), gross metastatic burden was decreased significantly in the BIBF 1120-treated groups, compared to control. In the HPAF-II model, there were an average of 7 metastatic events in the control animals compared to 0, 1 and 0 in the BIBF 1120, gemcitabine, and combination groups respectively ($p<0.001$ ANOVA, Fig. 2A). In the MIA PaCa-2 model, there were an average of 7 metastatic events in the control animals compared to 2, 4, and 2 in the BIBF 1120, gemcitabine, and combination groups respectively ($p<0.0001$ ANOVA). There was an additional decrease in metastatic events in the combination group in the MIA PaCa-2 study, compared to gemcitabine only ($p<0.0001$ Dunn's post-test, Fig. 2A).

In the AsPC-1 study, animals treated chronically with single agent BIBF 1120 also had a significantly reduced number of gross metastases compared to the control group ($p<0.0001$ student's *t-test*, Fig. 2A, B).

BIBF 1120 is a potent anti-angiogenic agent

BIBF 1120 inhibits the activity of multiple angiokinases (14); therefore, tumor sections from lung and pancreatic xenografts were assessed for microvessel density (MVD) and vascular function. MVD was determined using CD31 (PECAM-1). Sections were also stained for

Meca-32 (a pan-endothelial cell marker) and endomucin. Because these results closely resembled the CD31 data, the Meca-32 and endomucin data are not shown.

Tumor sections were also assessed for pericyte coverage, which has been implicated in resistance to anti-VEGF therapy (21, 22). Pericyte coverage was determined by co-localizing the pericyte marker NG2 with CD31. Similar results were confirmed with the co-localization of the pericyte marker (αSMA) with endomucin (data not shown). In lung xenografts, there was a substantial decrease in microvessel density and pericyte coverage (Fig. 3A, D, E) in BIBF 1120-treated animals. Chemotherapy alone had little effect on MVD or pericyte coverage.

We hypothesized that this decrease in MVD would negatively affect vascular perfusion, resulting in hypoxia and decrease in the blood flow into tumor tissue. We therefore performed functional staining with labeled dextrans, pimonidazole and doxorubicin to assess these parameters. Permeability and perfusion studies performed in A549-bearing SCID mice with labeled dextrans demonstrated a decrease in permeability of high molecular weight (FITC) dextran and perfusion of low molecular weight (Rhodamine) dextran (Figure 3B, F).

Pimonidazole is a 2-nitroimidazole that is reductively activated in hypoxic cells and forms stable adducts with thiol groups in proteins, peptides, and amino acids. Pimonidazole in these adducts was detected by immunohistochemistry (18, 23). Pimonidazole staining in H1993 (Fig. 3C, F) showed a significant increase in hypoxic areas after BIBF 1120 treatment concurrent with the decrease in MVD.

The MVD findings were similar in the pancreatic cancer xenografts. In MIA PaCa-2 xeongrafts, MVD was significantly decreased in BIBF 1120-treated groups compared to the control or chemotherapy groups ($p<0.0001$, Fig. 4A, D). These findings were also observed in the HPAF-II model (Fig. 4D). Due to the strong sensitivity of HPAF-II to gemcitabine tissue from gemcitabine-treated mice could not be analyzed. MVD analysis in AsPC-1 xenografts showed that BIBF 1120 reduces MVD within 5 days of treatment initiation ($p<0.001$, Fig. 4D), but was more pronounced after chronic treatment ($p<0.001$, Fig. 4D). Pericyte coverage in MIA PaCa-2 xenografts was similarly decreased by BIBF 1120 therapy (Fig. 4A, E). Additionally, in MIA PaCa-2 xenografts BIBF 1120 alone or in combination with gemcitabine dramatically elevated hypoxia (Fig. 4B, F).

To investigate the effect of BIBF 1120 on drug delivery, AsPC-1-bearing mice treated acutely (5 days) or chronically with BIBF 1120 were perfused intravenously with the naturally fluorescing chemotherapeutic agent doxorubicin (24) (Fig. 4C, G). In BIBF 1120 treated mice, the perfusion of tumor tissue with doxorubicin was decreased significantly compared to the control group in the acute ($p<0.01$) and chronic ($p<0.05$) treatment groups, with a more pronounced effect after chronic treatment (Fig. 4G).

BIBF 1120 does not promote an invasive phenotype

It has been reported that anti-angiogenic therapy may promote a more invasive phenotype (25–27). The mechanism underlying this phenotypic change is not fully elucidated but is thought to involve hypoxia-induced epithelial-mesenchymal transition (EMT) (28–31). To investigate whether the BIBF 1120-mediated hypoxia promoted a more invasive phenotype in our models, tissues from the lung and pancreatic cancer models were stained with canonical markers of EMT. A549 xenografts from each treatment group were evaluated for the expression of E-cadherin and vimentin. The level of E-cadherin, a marker of epithelial cells, was not affected by chemotherapy but was elevated by BIBF 1120 (Fig. 5A, C). While the level of vimentin, a mesenchymal marker, was unchanged compared to control in animals receiving single agent BIBF 1120 therapy but was decreased by combination

therapy in A549 xenografts (Fig. 5B, C). We also evaluated fibroblast recruitment, which is a component of EMT and invasion. Mature myofibroblasts were determined by α-SMA (Fig. 5B) and S100A4 staining (data not shown). αSMA levels were significantly decreased in BIBF 1120-treated animals bearing A549 xenografts (Fig. 5C, data not shown for Calu-6 and H1993).

We also investigated EMT in MIA PaCa-2 xenografts. We found that the expression of zeb1, a transcription factor that can induce EMT (32), did not differ across the four treatment groups nor did levels of vimentin or E-cadherin (Figure 6A, C, D). Additionally, β-catenin, a marker that shows membranous staining in epithelial cells and is transported to the nucleus in mesenchymal cells (33) did not differ significantly across groups (data not shown) in MIA PaCa-2 xenografts. Furthermore, BIBF 1120 reduced the expression level of αSMA in MIA PaCA-2 xenografts similar to the results in A549 tumors (Fig. 6B, D).

Discussion

Anti-angiogenic therapies—including anti-VEGF monoclonal antibodies and VEGFR TKIs—are currently FDA approved for lung, colorectal, kidney, thyroid, and brain cancer, as well as sarcomas. However, in many instances clinical of these drugs use has been fraught with toxicities, lack of predictive biomarkers, resistance, and only modest clinical benefit. The addition of bevacizumab to chemotherapy does not improve overall survival in advanced pancreatic cancer (5, 34, 35). While, in advanced non-squamous NSCLC, bevacizumab contributes a modest survival benefit when combined with carboplatin-paclitaxel, but not when combined with such other regimens as cisplatin-gemcitabine or erlotinib (2, 3, 36, 37). Numerous phase 3 trials have shown that adding VEGFR TKIs (sunitinib, sorafenib, vandetanib, and cediranib) to chemotherapy does not extend survival (4, 38, 39), despite promising results in pre-clinical, phase I, and phase II studies.

These disappointing results may be due to intrinsic or evasive resistance. Evasive resistance may arise from phenotypic changes due to EMT driven by hypoxia, a consequence of effective anti-angiogenic therapy. In the present study, we show that BIBF 1120, a triple angiokinase inhibitor of VEGFR, PDGFR, and FGFR, blunts primary tumor growth and metastasis, reduces microvessel density and fibroblast activation, induces hypoxia, but does not promote EMT in multiple preclinical models of lung and pancreatic cancer.

EMT predicts poor prognosis, promotes metastasis, and is associated with resistance to therapy (40, 41). Because hypoxia is a known driver of EMT (42) and we observed extensive hypoxia in BIBF 1120-treated tumors, we anticipated EMT induction as a possible limitation of the drug. However, we observed no evidence of EMT after evaluating of the expression of accepted markers of EMT. Instead, in A549 tumors, we observed reversal of EMT and promotion of an epithelial phenotype after BIBF 1120 treatment.

These effects may be due to the multi-targeted nature of BIBF 1120, which inhibits FGFR and PDGFR as well as VEGFR. Therapeutic strategies targeting the VEGF-VEGFR axis exclusively have been implicated in EMT induction in other malignancies (43). The absence of EMT in this study might be attributed to BIBF 1120 inhibition of fibroblast function, which has been implicated in regulating tumor cell phenotype (Ostapoff et al submitted). Consistent with this hypothesis, we observed a decrease in the level of αSMA^+ and $S100A4^+$ fibroblasts in tumors from BIBF 1120-treated animals. Alternatively, FGF pathway activation may provide an escape mechanism from VEGF-targeted strategies. For example, FGF signaling is activated in response to anti-VEGF therapy in glioblastoma multiforme (8, 44) and renal cell carcinoma (45). Furthermore, dual VEGF/FGF inhibition with the tyrosine kinase inhibitor brivanib demonstrates activity against pancreatic

neuroendocrine tumors that develop evasive resistance to anti-VEGF therapy (12). Additionally, stromal and tumor cell PDGFR targeting inhibits tumor growth and enhances the effect of chemotherapy in preclinical lung cancer models (9). Furthermore, targeted inhibition of VEGFR expressed on endothelial cells and PDGFR on pericytes provided enhanced therapeutic activity compared to the usage of either inhibitor as a single agent in pancreatic islet cell carcinoma (6). Similarly, we found that BIBF 1120, which inhibits pathways associated with endothelial and pericyte function, decreased pericyte coverage. This is in contrast to the concept of anti-angiogenic induction of vascular normalization. Consistent with a decrease in vascular function, we observed decreased delivery doxorubicin in AsPC-1 tumors after acute or chronic therapy with BIBF 1120. These results are consistent with recent clinical data that show a rapid decrease in the delivery of docetaxel after treatment with bevacizumab (46, 47).

To date, a number of BIBF 1120 clinical studies have been reported, including combination studies with standard lung cancer chemotherapy regimens (carboplatin-paclitaxel and single-agent pemetrexed) (48, 49). Based on encouraging safety and efficacy data, two phase 3 trials (LUME-Lung 1 [NCT00805194] and LUME-Lung 2 [NCT00806819]) evaluating BIBF 1120 in combination with docetaxel and pemetrexed have been performed.

Other strategies targeting VEGF/PDGF/FGF have demonstrated efficacy in preclinical cancer models (50). Our study supports this strategy and, for the first time, examines its efficacy and biological effects in combination with standard chemotherapy. Additionally, to our knowledge, this is the first study to examine the impact of multi-targeted angiokinase inhibition on EMT. In conjunction with encouraging clinical safety and efficacy data, these findings warrant further clinical investigation of this agent, including ongoing trials in lung cancer and further development in pancreatic cancer.

Supplementary Material

Refer to Web version on PubMed Central for supplementary material.

Acknowledgments

Financial Support: This work was supported in part by a sponsored research agreement from Boerhringer Ingelheim, Inc., (to D.E. Gerber and R.A. Brekken), NCI SPORE P50CA70907 (to R.A. Brekken) and the Effie Marie Cain Scholarship in Angiogenesis Research (to R.A. Brekken).

We thank Jason Toombs for technical assistance and Drs. Joan Schiller and John Minna and members of the Brekken lab for advice and thoughtful discussion. We also thank Dr. Frank Hilberg for provision of BIBF 1120 and support.

References

1. Bergers G, Hanahan D. Modes of resistance to anti-angiogenic therapy. Nat Rev Cancer. 2008; 8:592–603. [PubMed: 18650835]
2. Sandler A, Gray R, Perry MC, Brahmer J, Schiller JH, Dowlati A, et al. Paclitaxel-carboplatin alone or with bevacizumab for non-small-cell lung cancer. N Engl J Med. 2006; 355:2542–50. [PubMed: 17167137]
3. Reck M, von Pawel J, Zatloukal P, Ramlau R, Gorbounova V, Hirsh V, et al. Phase III trial of cisplatin plus gemcitabine with either placebo or bevacizumab as first-line therapy for nonsquamous non-small-cell lung cancer: AVAil. J Clin Oncol. 2009; 27:1227–34. [PubMed: 19188680]
4. Scagliotti G, Novello S, von Pawel J, Reck M, Pereira JR, Thomas M, et al. Phase III study of carboplatin and paclitaxel alone or with sorafenib in advanced non-small-cell lung cancer. J Clin Oncol. 2010; 28:1835–42. [PubMed: 20212250]

5. Kindler HL, Niedzwiecki D, Hollis D, Sutherland S, Schrag D, Hurwitz H, et al. Gemcitabine plus bevacizumab compared with gemcitabine plus placebo in patients with advanced pancreatic cancer: phase III trial of the Cancer and Leukemia Group B (CALGB 80303). J Clin Oncol. 2010; 28:3617–22. [PubMed: 20606091]
6. Bergers G, Song S, Meyer-Morse N, Bergsland E, Hanahan D. Benefits of targeting both pericytes and endothelial cells in the tumor vasculature with kinase inhibitors. J Clin Invest. 2003; 111:1287–95. [PubMed: 12727920]
7. Erber R, Thurnher A, Katsen AD, Groth G, Kerger H, Hammes HP, et al. Combined inhibition of VEGF and PDGF signaling enforces tumor vessel regression by interfering with pericyte-mediated endothelial cell survival mechanisms. FASEB J. 2004; 18:338–40. [PubMed: 14657001]
8. Casanovas O, Hicklin DJ, Bergers G, Hanahan D. Drug resistance by evasion of antiangiogenic targeting of VEGF signaling in late-stage pancreatic islet tumors. Cancer Cell. 2005; 8:299–309. [PubMed: 16226705]
9. Gerber DE, Gupta P, Dellinger MT, Toombs JE, Peyton M, Duignan I, et al. Stromal platelet-derived growth factor receptor alpha (PDGFRalpha) provides a therapeutic target independent of tumor cell PDGFRalpha expression in lung cancer xenografts. Mol Cancer Ther. 2012; 11:2473–82. [PubMed: 22933705]
10. Donnem T, Al-Shibli K, Al-Saad S, Busund LT, Bremnes RM. Prognostic impact of fibroblast growth factor 2 in non-small cell lung cancer: coexpression with VEGFR-3 and PDGF-B predicts poor survival. J Thorac Oncol. 2009; 4:578–85. [PubMed: 19318994]
11. Kuwahara K, Sasaki T, Kuwada Y, Murakami M, Yamasaki S, Chayama K. Expressions of angiogenic factors in pancreatic ductal carcinoma: a correlative study with clinicopathologic parameters and patient survival. Pancreas. 2003; 26:344–9. [PubMed: 12717266]
12. Allen E, Walters IB, Hanahan D. Brivanib, a dual FGF/VEGF inhibitor, is active both first and second line against mouse pancreatic neuroendocrine tumors developing adaptive/evasive resistance to VEGF inhibition. Clin Cancer Res. 2011; 17:5299–310. [PubMed: 21622725]
13. Kono SA, Marshall ME, Ware KE, Heasley LE. The fibroblast growth factor receptor signaling pathway as a mediator of intrinsic resistance to EGFR-specific tyrosine kinase inhibitors in non-small cell lung cancer. Drug Resist Updat. 2009; 12:95–102. [PubMed: 19501013]
14. Hilberg F, Roth GJ, Krssak M, Kautschitsch S, Sommergruber W, Tontsch-Grunt U, et al. BIBF 1120: triple angiokinase inhibitor with sustained receptor blockade and good antitumor efficacy. Cancer Res. 2008; 68:4774–82. [PubMed: 18559524]
15. Kudo K, Arao T, Tanaka K, Nagai T, Furuta K, Sakai K, et al. Antitumor activity of BIBF 1120, a triple angiokinase inhibitor, and use of VEGFR2+pTyr+ peripheral blood leukocytes as a pharmacodynamic biomarker in vivo. Clin Cancer Res. 2011; 17:1373–81. [PubMed: 21131553]
16. Dineen SP, Roland CL, Greer R, Carbon JG, Toombs JE, Gupta P, et al. Smac mimetic increases chemotherapy response and improves survival in mice with pancreatic cancer. Cancer Res. 2010; 70:2852–61. [PubMed: 20332237]
17. Dineen SP, Lynn KD, Holloway SE, Miller AF, Sullivan JP, Shames DS, et al. Vascular endothelial growth factor receptor 2 mediates macrophage infiltration into orthotopic pancreatic tumors in mice. Cancer Res. 2008; 68:4340–6. [PubMed: 18519694]
18. Arnold SA, Rivera LB, Miller AF, Carbon JG, Dineen SP, Xie Y, et al. Lack of host SPARC enhances vascular function and tumor spread in an orthotopic murine model of pancreatic carcinoma. Dis Model Mech. 2010; 3:57–72. [PubMed: 20007485]
19. Sullivan LA, Carbon JG, Roland CL, Toombs JE, Nyquist-Andersen M, Kavlie A, et al. r84, a novel therapeutic antibody against mouse and human VEGF with potent anti-tumor activity and limited toxicity induction. PLoS One. 2010; 5:e12031. [PubMed: 20700512]
20. Greer RM, Peyton M, Larsen JE, Girard L, Xie Y, Gazdar AF, et al. SMAC mimetic (JP1201) sensitizes non-small cell lung cancers to multiple chemotherapy agents in an IAP-dependent but TNF-alpha-independent manner. Cancer Res. 2011; 71:7640–8. [PubMed: 22049529]
21. Benjamin LE, Golijanin D, Itin A, Pode D, Keshet E. Selective ablation of immature blood vessels in established human tumors follows vascular endothelial growth factor withdrawal. J Clin Invest. 1999; 103:159–65. [PubMed: 9916127]

22. Nisancioglu MH, Betsholtz C, Genove G. The absence of pericytes does not increase the sensitivity of tumor vasculature to vascular endothelial growth factor-A blockade. Cancer Res. 2010; 70:5109–15. [PubMed: 20501841]
23. Raleigh JA, Koch CJ. Importance of thiols in the reductive binding of 2-nitroimidazoles to macromolecules. Biochem Pharmacol. 1990; 40:2457–64. [PubMed: 2176499]
24. Egorin MJ, Hildebrand RC, Cimino EF, Bachur NR. Cytofluorescence localization of adriamycin and daunorubicin. Cancer Res. 1974; 34:2243–5. [PubMed: 4843531]
25. Birner P, Schindl M, Obermair A, Plank C, Breitenecker G, Oberhuber G. Overexpression of hypoxia-inducible factor 1alpha is a marker for an unfavorable prognosis in early-stage invasive cervical cancer. Cancer Res. 2000; 60:4693–6. [PubMed: 10987269]
26. Vaupel P, Kelleher DK, Hockel M. Oxygen status of malignant tumors: pathogenesis of hypoxia and significance for tumor therapy. Semin Oncol. 2001; 28:29–35. [PubMed: 11395850]
27. Bos R, van der Groep P, Greijer AE, Shvarts A, Meijer S, Pinedo HM, et al. Levels of hypoxia-inducible factor-1alpha independently predict prognosis in patients with lymph node negative breast carcinoma. Cancer. 2003; 97:1573–81. [PubMed: 12627523]
28. Yoo YG, Christensen J, Gu J, Huang LE. HIF-1alpha mediates tumor hypoxia to confer a perpetual mesenchymal phenotype for malignant progression. Sci Signal. 2011; 4(pt4)
29. Lester RD, Jo M, Montel V, Takimoto S, Gonias SL. uPAR induces epithelial-mesenchymal transition in hypoxic breast cancer cells. J Cell Biol. 2007; 178:425–36. [PubMed: 17664334]
30. Yang MH, Wu MZ, Chiou SH, Chen PM, Chang SY, Liu CJ, et al. Direct regulation of TWIST by HIF-1alpha promotes metastasis. Nat Cell Biol. 2008; 10:295–305. [PubMed: 18297062]
31. Carbone C, Moccia T, Zhu C, Paradiso G, Budillon A, Chiao PJ, et al. Anti-VEGF treatment-resistant pancreatic cancers secrete proinflammatory factors that contribute to malignant progression by inducing an EMT cell phenotype. Clin Cancer Res. 2011; 17:5822–32. [PubMed: 21737511]
32. Vandewalle C, Van Roy F, Berx G. The role of the ZEB family of transcription factors in development and disease. Cell Mol Life Sci. 2009; 66:773–87. [PubMed: 19011757]
33. Sanchez-Tillo E, de Barrios O, Siles L, Cuatrecasas M, Castells A, Postigo A. beta-catenin/TCF4 complex induces the epithelial-to-mesenchymal transition (EMT)-activator ZEB1 to regulate tumor invasiveness. Proc Natl Acad Sci U S A. 2011; 108:19204–9. [PubMed: 22080605]
34. Van Cutsem E, Vervenne WL, Bennouna J, Humblet Y, Gill S, Van Laethem JL, et al. Phase III trial of bevacizumab in combination with gemcitabine and erlotinib in patients with metastatic pancreatic cancer. J Clin Oncol. 2009; 27:2231–7. [PubMed: 19307500]
35. Astsaturov IA, Meropol NJ, Alpaugh RK, Burtness BA, Cheng JD, McLaughlin S, et al. Phase II and coagulation cascade biomarker study of bevacizumab with or without docetaxel in patients with previously treated metastatic pancreatic adenocarcinoma. Am J Clin Oncol. 2011; 34:70–5. [PubMed: 20458210]
36. Johnson DH, Fehrenbacher L, Novotny WF, Herbst RS, Nemunaitis JJ, Jablons DM, et al. Randomized phase II trial comparing bevacizumab plus carboplatin and paclitaxel with carboplatin and paclitaxel alone in previously untreated locally advanced or metastatic non-small-cell lung cancer. J Clin Oncol. 2004; 22:2184–91. [PubMed: 15169807]
37. Herbst RS, Ansari R, Bustin F, Flynn P, Hart L, Otterson GA, et al. Efficacy of bevacizumab plus erlotinib versus erlotinib alone in advanced non-small-cell lung cancer after failure of standard first-line chemotherapy (BeTa): a double-blind, placebo-controlled, phase 3 trial. Lancet. 2011; 377:1846–54. [PubMed: 21621716]
38. Scagliotti GV, Krzakowski M, Szczesna A, Strausz J, Makhson A, Reck M, et al. Sunitinib plus erlotinib versus placebo plus erlotinib in patients with previously treated advanced non-small-cell lung cancer: a phase III trial. J Clin Oncol. 2012; 30:2070–8. [PubMed: 22564989]
39. Herbst RS, Sun Y, Eberhardt WE, Germonpre P, Saijo N, Zhou C, et al. Vandetanib plus docetaxel versus docetaxel as second-line treatment for patients with advanced non-small-cell lung cancer (ZODIAC): a double-blind, randomised, phase 3 trial. Lancet Oncol. 2010; 11:619–26. [PubMed: 20570559]
40. Rhim AD, Mirek ET, Aiello NM, Maitra A, Bailey JM, McAllister F, et al. EMT and dissemination precede pancreatic tumor formation. Cell. 2012; 148:349–61. [PubMed: 22265420]

41. Yauch RL, Januario T, Eberhard DA, Cavet G, Zhu W, Fu L, et al. Epithelial versus mesenchymal phenotype determines in vitro sensitivity and predicts clinical activity of erlotinib in lung cancer patients. Clin Cancer Res. 2005; 11:8686–98. [PubMed: 16361555]

42. Peinado H, Cano A. A hypoxic twist in metastasis. Nat Cell Biol. 2008; 10:253–4. [PubMed: 18311179]

43. Mak P, Leav I, Pursell B, Bae D, Yang X, Taglienti CA, et al. ERbeta impedes prostate cancer EMT by destabilizing HIF-1alpha and inhibiting VEGF-mediated snail nuclear localization: implications for Gleason grading. Cancer Cell. 2010; 17:319–32. [PubMed: 20385358]

44. Paez-Ribes M, Allen E, Hudock J, Takeda T, Okuyama H, Vinals F, et al. Antiangiogenic therapy elicits malignant progression of tumors to increased local invasion and distant metastasis. Cancer Cell. 2009; 15:220–31. [PubMed: 19249680]

45. Fernando NT, Koch M, Rothrock C, Gollogly LK, D'Amore PA, Ryeom S, et al. Tumor escape from endogenous, extracellular matrix-associated angiogenesis inhibitors by up-regulation of multiple proangiogenic factors. Clin Cancer Res. 2008; 14:1529–39. [PubMed: 18316578]

46. Casanovas O. Cancer: Limitations of therapies exposed. Nature. 2012; 484:44–6. [PubMed: 22481354]

47. Van der Veldt AA, Lubberink M, Bahce I, Walraven M, de Boer MP, Greuter HN, et al. Rapid decrease in delivery of chemotherapy to tumors after anti-VEGF therapy: implications for scheduling of anti-angiogenic drugs. Cancer Cell. 2012; 21:82–91. [PubMed: 22264790]

48. Ellis PM, Kaiser R, Zhao Y, Stopfer P, Gyorffy S, Hanna N. Phase I open-label study of continuous treatment with BIBF 1120, a triple angiokinase inhibitor, and pemetrexed in pretreated non-small cell lung cancer patients. Clin Cancer Res. 2010; 16:2881–9. [PubMed: 20460487]

49. Doebele RC, Conkling P, Traynor AM, Otterson GA, Zhao Y, Wind S, et al. A phase I, open-label dose-escalation study of continuous treatment with BIBF 1120 in combination with paclitaxel and carboplatin as first-line treatment in patients with advanced non-small-cell lung cancer. Ann Oncol. 2012

50. Taeger J, Moser C, Hellerbrand C, Mycielska ME, Glockzin G, Schlitt HJ, et al. Targeting FGFR/PDGFR/VEGFR impairs tumor growth, angiogenesis, and metastasis by effects on tumor cells, endothelial cells, and pericytes in pancreatic cancer. Mol Cancer Ther. 2011; 10:2157–67. [PubMed: 21885862]

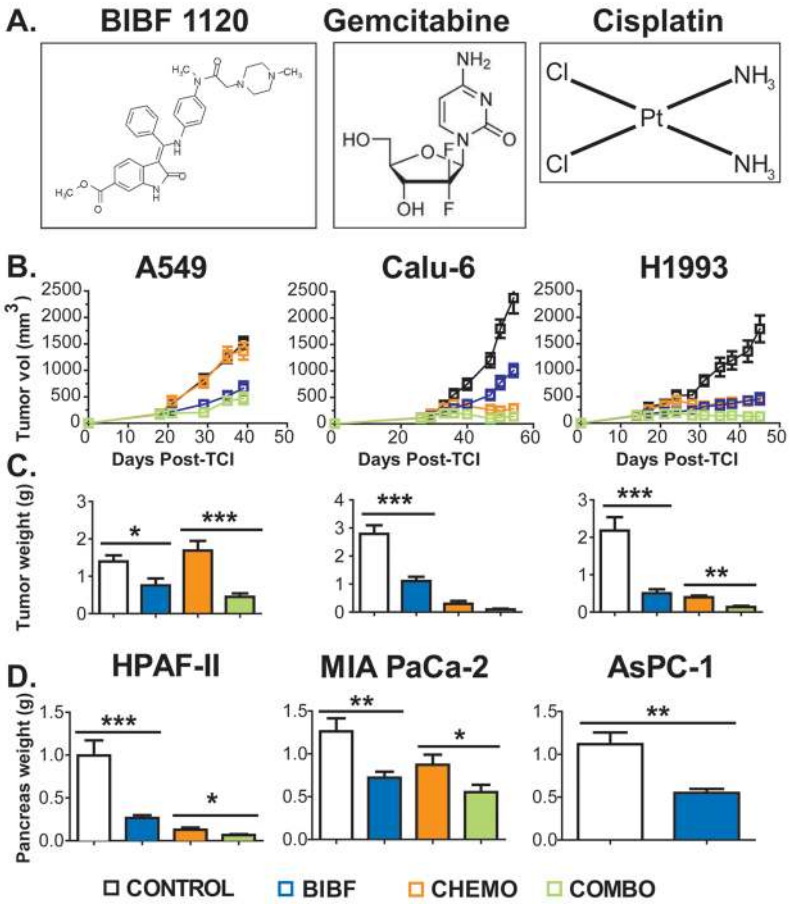

Figure 1. BIBF 1120 inhibits primary tumor growth in subcutaneous lung and orthotopic pancreatic cancer xenografts

A) Chemical structures of BIBF 1120 (first panel) and chemotherapeutics Gemcitabine and Cisplatin (second and third panels). **B**) The indicted NSCLC cells were injected subcutaneously into mice. Treatment by with vehicle (Control), BIBF 1120 (BIBF, 50 mg/kg, daily), CHEMO (gemcitabine [25 mg/kg 2x/week] + Cisplatin [1 mg/kg 1x/week]) was initiated when average tumor volume reached 100–150 mm^3 (n=10/group). Tumor growth curves displaying mean tumor volume +/− SEM and **C)** mean final tumor weights +/− SEM are shown. **D**) The indicated pancreatic cancer cells were injected orthotopically into SCID mice. Treatment was initiated 7–10 days post tumor cell injection (TCI). Animals were treated as above with the exception of chemotherapy; gemcitabine was given at 12.5 mg/kg 3x/week. Mean final pancreas weight +/− SEM is shown (n=10/group). *, p<0.05; **, p<0.01; ***, p<0.001; ****, p<0.0001 by Dunn's post-test.

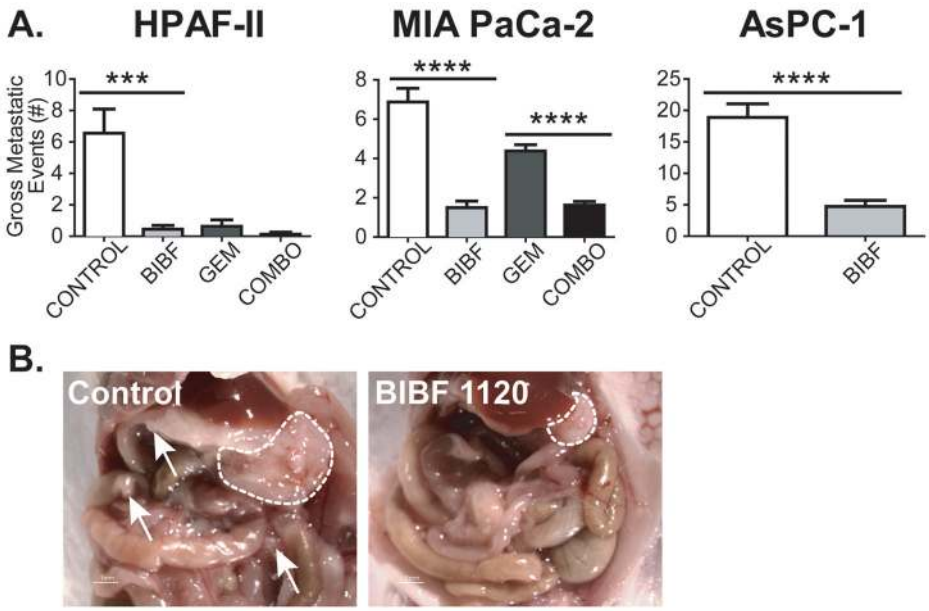

Figure 2. BIBF 1120 decreases gross metastatic burden in orthotopic pancreatic xenografts

A) At sacrifice, the number of gross metastatic events was recorded. Gross metastatic burden was decreased significantly in BIBF 1120-treated animals compared to control groups in each model. **B**) Representative image of a HPAF-II tumor presentation at the time of sacrifice. Dashed lines, primary tumor borders; Arrows, metastatic foci. Bar graphs indicate mean + SEM. ***, $p<0.001$; ****, $p<0.0001$ by student's t-test / Dunn's post-test.

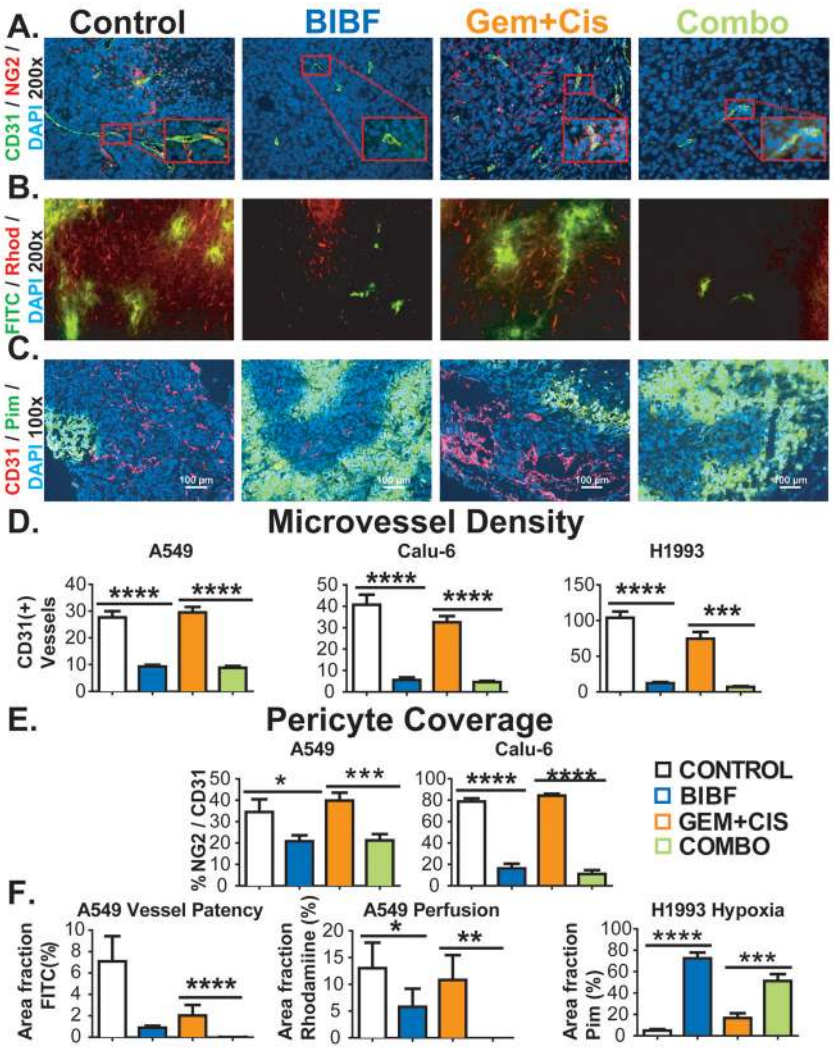

Figure 3. BIBF 1120 shows potent anti-angiogenic effects, decreases perfusion and induces hypoxia in lung cancer xenografts

Vascular parameters of NSCLC tumors were evaluated by immunohistochemistry and perfusion studies. **A**) Representative images of microvessel density (CD31) and pericyte coverage (NG2) in Calu-6 xenografts at 200x magnification (inset: 400x), with DAPI labeling nuclei. **B**) Representative images of perfusion of high molecular weight (FITC, MW: 2 million) and low molecular weight (Rhodamine, MW 10000) dextrans in A549 xenografts. **C**) Representative images of hypoxia as assessed by pimonidazole staining in H1993 xenografts. Scale bar, 100 μm. Quantification of microvessel density (**D**), pericyte coverage (**E**) and dextran perfusion data and hypoxia (**F**). Vessel patency reflects signal from high molecular weight dextran and perfusion reflects signal from low molecular weight dextran. Bar graphs indicate means + SEM. A minimum of 5 images were acquired per group. Results were given as mean percentage of thresholded area or absolute vessel counts per 200x field. *, $p<0.05$; **, $p<0.01$; ***, $p<0.001$; ****, $p<0.0001$ by Dunn's post-test.

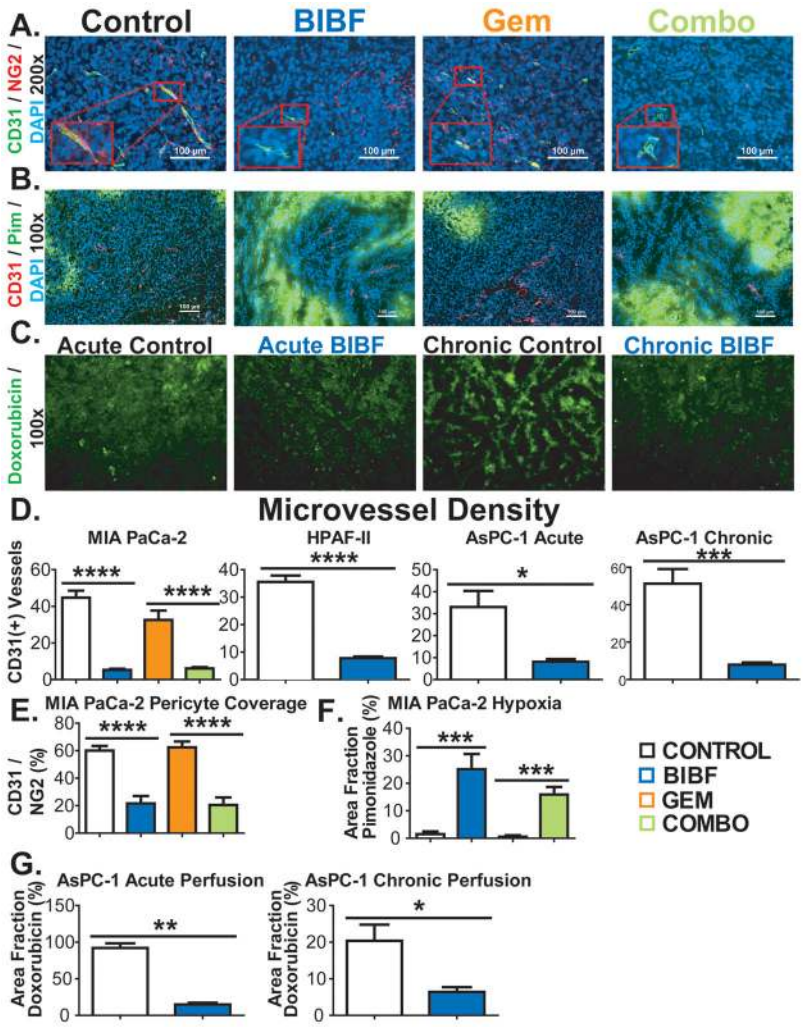

Figure 4. BIBF 1120 shows potent anti-angiogenic effects, induces hypoxia and decreases drug delivery in pancreatic cancer xenografts

Vascular parameters of pancreatic tumors were evaluated by immunohistochemistry and perfusion studies. **A**) Representative images of microvessel density (CD31) and pericyte coverage (NG2) in Mia PaCa-2 xenografts at 200x magnification (inset: 400x), with DAPI labeling nuclei. Scale bar, 100 μm. **B**) Representative images of CD31 and pimonidazole reactivity in MIA PaCa-2 xenografts. Scale bar, 100 μm. **C**) Representative images of doxorubicin perfusion in AsPC-1 xenografts after acute or chronic exposure to BIBF 1120. Quantification of microvessel density (**D**)**,** pericyte coverage (**E**), hypoxia (**F**)**,** and doxorubicin (perfusion) fluorescence (**G**) is shown. Bar graphs indicate means + SEM. A minimum of 5 images were acquired per group. Results are mean percentage of thresholded area or absolute vessel counts per field. *, $p<0.05$; **, $p<0.01$; ***, $p<0.001$; ****, $p<0.0001$ by Dunn's post-test.

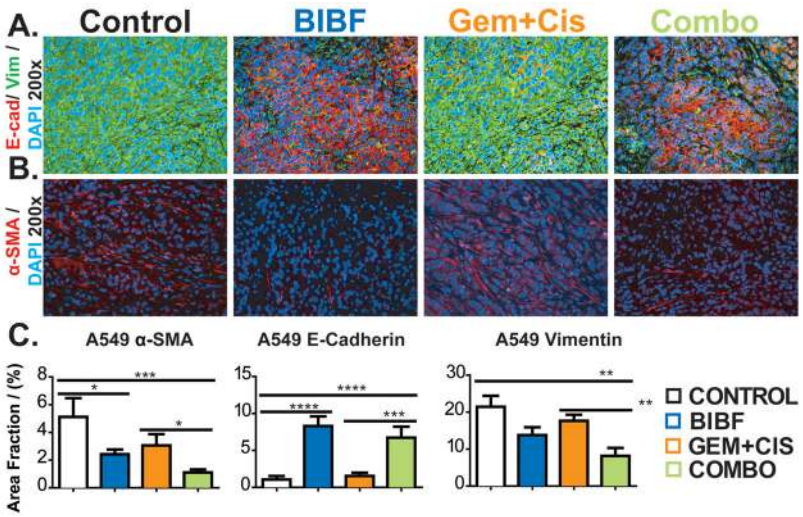

Figure 5. BIBF 1120 does not drive an invasive phenotype in lung cancer

EMT markers from lung tumors were evaluated by immunohistochemistry. **A**) Representative images of mature myofibroblasts (α-SMA) at 200x magnification with DAPI labeling nuclei. **B**) Representative images of E-cadherin and vimentin at 200x magnification. **C**) Quantification of fibroblasts, E-cadherin and vimentin. Bar graphs indicate mean +/− SEM. A minimum of 5 images were acquired per group. Results were given as mean percentage of thresholded area per field. *, $p<0.05$; **, $p<0.01$; ***, $p<0.001$; ****, $p<0.0001$ by Dunn's post-test.

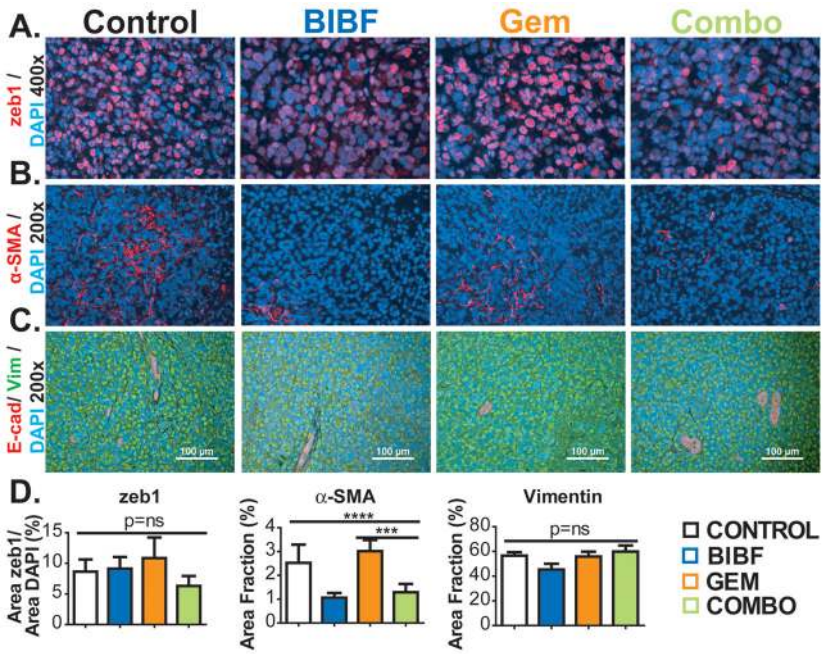

Figure 6. BIBF 1120 does not drive an invasive phenotype in pancreatic cancer

EMT markers from pancreatic tumors were evaluated by immunohistochemistry. **A**) Representative images of zeb1 at 200x magnification with DAPI labeling nuclei. **B**) Representative images of mature myofibroblasts (α-SMA) at 200x magnification with DAPI labeling nuclei. **C**) Representative images of E-cadherin and vimentin at 200x magnification. Scale bar, 100 μm. **D**) Quantification of zeb1, fibroblasts, E-cadherin and vimentin. Bar graphs indicate means +/− SEM. A minimum of 5 images were acquired per group. Results were given as mean percentage of thresholded area per field. *, $p<0.05$; **, $p<0.01$; ***, $p<0.001$; ****, $p<0.0001$ by Dunn's post-test.